

1 **West Antarctic ice loss influenced by anthropogenic forcing and internal**  
2 **climate variability**

3 Paul R. Holland<sup>1\*</sup>, Thomas J. Bracegirdle<sup>1</sup>, Pierre Dutrieux<sup>2</sup>, Adrian Jenkins<sup>1</sup>, and Eric J. Steig<sup>3</sup>

4 <sup>1</sup>British Antarctic Survey, Cambridge, UK

5 <sup>2</sup>Lamont-Doherty Earth Observatory of Columbia University, Palisades, NY, USA

6 <sup>3</sup>Department of Earth and Space Sciences, University of Washington, Seattle, WA, USA

7 \*corresponding author

8

9 **Recent ice loss from the West Antarctic Ice Sheet has been caused by ocean melting of ice**  
10 **shelves in the Amundsen Sea. Eastward wind anomalies at the shelf break enhance the**  
11 **import of warm Circumpolar Deep Water onto the Amundsen Sea continental shelf, which**  
12 **creates transient melting anomalies with an approximately decadal period. No**  
13 **anthropogenic influence on this process has been established. Here, we combine**  
14 **observations and climate model simulations to suggest that increased greenhouse-gas**  
15 **forcing caused shelf-break winds to transition from mean easterlies in the 1920s to the**  
16 **near-zero mean zonal winds of the present day. Strong internal climate variability, primarily**  
17 **linked to the tropical Pacific, is superimposed upon this forced trend. We infer that the**  
18 **Amundsen Sea experienced decadal ocean variability throughout the 20<sup>th</sup> century, with**  
19 **warm anomalies gradually becoming more prevalent, offering a credible explanation for**  
20 **the ongoing ice loss. Existing climate model projections show that strong future**  
21 **greenhouse-gas forcing creates persistent mean westerly shelf-break winds by 2100,**  
22 **suggesting a further enhancement of warm ocean anomalies. These wind changes are**  
23 **weaker under a scenario in which greenhouse gases are stabilised.**

24 The West Antarctic Ice Sheet (WAIS) has been losing ice throughout the satellite record,  
25 currently at a rate equivalent to global sea-level rise of  $\sim 4.5$  cm/century (2012-2017 average)<sup>1</sup>.  
26 This ice loss is known to be driven by changes in ocean melting of ice shelves<sup>2</sup>, but it remains  
27 unclear whether these changes can be attributed to contemporary climate change. The rate  
28 of ice loss shows large variations<sup>3,4</sup> driven by decadal variability in oceanic conditions<sup>5,6</sup>.  
29 However, this ocean variability does not necessarily explain the overall ice loss, since on  
30 longer timescales the WAIS could be in balance with decadal-varying forcing<sup>7</sup>. There is  
31 evidence that historical ocean melting anomalies caused ice streams to unground from  
32 stabilising seabed features, triggering geometrical ice and ocean feedbacks that remain  
33 active<sup>6,8-12</sup>. In this study, we consider the possibility that the decadal variability is  
34 superimposed on a longer-term trend, increasing the mean melt rates about which decadal  
35 variations occur.

36

37 Warm Circumpolar Deep Water (CDW) has occupied the Amundsen Sea continental shelf  
38 since the earliest observations<sup>13</sup> but the thickness of the CDW layer varies markedly, driving  
39 the decadal variability in melting<sup>6,14</sup>. Observational and modelling evidence shows that the  
40 transport of CDW onto the Amundsen Sea shelf is strongly affected by ocean surface stresses  
41 at the shelf break<sup>5,6,14-18</sup>. By modifying the barotropic ocean flow, eastward stress anomalies  
42 enhance an undercurrent that transports CDW on-shelf via seabed troughs, thickening the  
43 CDW layer and increasing melting<sup>5,18,19</sup>. Additional processes such as local sea-ice growth and  
44 wind forcing modify ocean conditions over the shelf<sup>20-22</sup>. However, these surface processes  
45 have less influence at greater depths, which dominate variability in ice-shelf melting, and on  
46 longer timescales, which are of greatest importance to the ice-sheet response<sup>7</sup>. Furthermore,  
47 local surface processes can only reduce or re-distribute the ocean heat on the shelf; CDW

48 import is the only process that can increase the overall on-shelf heat content. As a result, the  
49 observed history of ice-shelf melting shows a close correspondence to the import of CDW  
50 onto the shelf, which is regulated by zonal surface stresses over the shelf break<sup>5,6</sup>. This study  
51 relies on this established linkage between winds and ice-shelf melting and examines the wider  
52 drivers of wind anomalies, including tropical Pacific linkages, 20<sup>th</sup>-century variability, the role  
53 of anthropogenic forcing, and future projections.

54

### 55 **Tropical Pacific forcing of Amundsen Sea variability**

56 We estimate the total ocean surface stress on the Amundsen Sea, accounting for the effect  
57 of sea ice, by combining wind data from the ERA-Interim reanalysis with satellite-tracked sea  
58 ice drift observations (Methods; ref. <sup>23</sup>). The Amundsen Sea shelf break sits near the centre of  
59 the Amundsen Sea Low<sup>24</sup>, where the long-term mean zonal stress is negligible (Figure 1a).  
60 Interannual stress variability is large (Figure 1b), and its uniformity across the region implies  
61 that shelf-break stresses experience exceptionally high variability relative to their low mean.  
62 This may explain why strong ocean (and ice sheet) variability occurs in the Amundsen Sea.

63

64 Total stress and wind-only stress differ substantially over the shelf, but are highly correlated  
65 at the shelf break (Supplementary Figure S1). Therefore, throughout this study we use zonal  
66 winds over the Pine Island/Thwaites Troughs (PITT; Figure 1a) as a proxy for zonal stress and  
67 hence CDW transport onto the shelf. PITT winds contain anomalies with an approximately  
68 decadal period (Figure 2a), which dominate the variability in ice-sheet forcing<sup>5,6</sup>. To focus  
69 upon this variability, we hereafter apply a 2-year running mean to all quantities, isolating  
70 decadal anomalies while preserving their extrema (Supplementary Figure S2).

71

72 Maps of correlation between PITT winds and global sea-surface temperature (SST) and sea-  
73 level pressure (SLP) are shown in Figure 2b and Supplementary Figure S3. Eastward wind  
74 anomalies are associated with weakening of the Amundsen Sea Low, part of a global response  
75 to anomalies in the tropical Pacific that is transmitted by standing atmospheric Rossby  
76 waves<sup>9,25</sup>. The global wind anomalies induce accompanying global SST anomalies by altering  
77 Ekman transport and surface fluxes<sup>26</sup>. Figure 2 also shows the Southern Oscillation Index  
78 (SOI), which represents the El Niño—Southern Oscillation, and the Interdecadal Pacific  
79 Oscillation (IPO) tripole index, which represents decadal Pacific variability (Methods). PITT  
80 winds are highly correlated with these indices, which represent natural variability that is  
81 internally generated within the climate system. Indeed, PITT wind anomalies are highly  
82 correlated to all measures of tropical Pacific variability<sup>9,14</sup>, and bear no relation to other  
83 climate indices (Supplementary Figure S4).

84

85 The strong statistical link between PITT winds and tropical Pacific SSTs provides an  
86 opportunity to constrain historical wind forcing of the Amundsen Sea, because tropical Pacific  
87 SSTs have been adequately observed since the 1920s (ref. <sup>26</sup>). To utilise these observations,  
88 we use an ensemble of ‘pacemaker’ climate model simulations<sup>27</sup> (PACE) to estimate PITT  
89 winds during the 20<sup>th</sup> century (Methods). PACE comprises 20 simulations of the Community  
90 Earth System Model (CESM) under natural and anthropogenic radiative forcings, but also  
91 constrained to follow observed tropical Pacific SST anomalies since 1920. This constraint  
92 ensures that the model winds follow the real history of the internal climate variability that is  
93 associated with the tropical Pacific. Since Pacific variability has such a strong influence on the  
94 Amundsen Sea, these simulations provide a constrained estimate of historical variability in  
95 PITT winds.

96

97 Each simulation within the PACE ensemble represents a single realisation of the climate, so  
98 the real winds can be considered as being comparable to an individual ensemble member.

99 The mean and variability of PITT winds in the PACE simulations compare very favourably with  
100 ERA-Interim (Figure 3a). The PACE ensemble mean represents the mean trajectory of PITT  
101 winds under the real historical radiative forcing and tropical Pacific SST evolution. This  
102 ensemble mean is arguably the best available reconstruction of historical PITT winds, since it  
103 averages over multiple realisations of the unknown internal climate variability associated with  
104 regions outside the tropical Pacific. Model correlation maps (Supplementary Figure S5)  
105 confirm that the PACE ensemble-mean winds follow the processes seen in the observations.

106

107 The PACE ensemble mean PITT winds show a general eastward trend, with eastward wind  
108 anomalies in 1940, the 1950s, 1970, and 1980 onwards (Figure 3a) that are consistent with  
109 the glacial history inferred from sediments<sup>12</sup> and remote sensing observations<sup>3,4,8</sup>. These  
110 linked wind and glacial anomalies are explored further below. The wind history is also  
111 supported by water-isotope ratios from West Antarctic ice cores, which show an increasing  
112 trend during the 20<sup>th</sup> century and anomalously high values in response to the major El Niño  
113 of the early 1940s (refs. <sup>28,29</sup>).

114

### 115 **The role of anthropogenic forcing**

116 The PACE ensemble mean contains both a radiatively-forced trend and the mean influence of  
117 internal variability associated with the tropical Pacific. We separate these by estimating the  
118 radiatively-forced trend from the CESM Large Ensemble<sup>30</sup> (LENS; Methods). LENS uses the  
119 same model as PACE but without tropical SST restoring, providing 40 different realisations of

120 internal climate variability from all sources, Pacific and otherwise (Figure 3c). Taking the  
121 ensemble mean of LENS averages out this random internal variability, isolating the radiatively  
122 forced trend. The LENS ensemble mean has a PITT zonal wind trend of  $\sim 0.5$  m/s/century  
123 during 1920—2005 (Table 1). Taken together, the CESM simulations (LENS and PACE)  
124 therefore imply that a forced wind trend removed a mean easterly PITT wind of  $\sim 0.5$  m/s that  
125 existed during the 1920s, to arrive at the present near-zero mean zonal winds (Figure 3a).  
126 Acceleration of the southern sub-polar westerlies is a well-known consequence of the  
127 meridional structure of radiatively forced atmospheric warming<sup>31,32</sup>. Our results show that  
128 this trend includes the latitude of PITT winds (Figure 4a), despite the low correlation between  
129 the sub-polar westerlies and PITT winds on interannual timescales (see the Southern Annular  
130 Mode in Supplementary Figures S2 and S4).

131

132 The PITT region is highly sensitive to the modelled pattern of trends in the sub-polar  
133 westerlies<sup>31</sup>. The wider ensemble of climate models contributing to the Coupled Model  
134 Intercomparison Project, phase 5 (CMIP5; Methods) includes a variety of historical trends.  
135 The CMIP5 ensemble has no mean trend (Table 1), so the CESM is an outlier in this regard.  
136 However, the CMIP5 simulations have large biases in mean PITT winds relative to ERA-Interim  
137 (Figure 4b, Supplementary Table S1), and the simulations with a smaller bias have a larger  
138 historical trend. The CESM simulations have an exceptionally small bias in mean PITT winds,  
139 providing support for their relatively large historical trends.

140

141 To formally separate tropical Pacific variability from the radiatively-forced trend, we combine  
142 the PACE and LENS ensembles. As described above, the LENS ensemble mean represents the  
143 radiatively-forced trend, while the PACE ensemble mean represents the radiatively-forced

144 trend plus the real tropical Pacific variability. Therefore, to isolate the influence of Pacific  
145 variability, we subtract the LENS ensemble mean ('forced response') from the PACE ensemble  
146 mean ('full response') to leave the 'tropical response'<sup>27</sup>, i.e. the influence of tropical Pacific  
147 SST restoring (Figure 3b). Tropical response winds closely follow the unfiltered IPO index  
148 (Methods), implying multi-decadal variability in PITT winds (e.g. filtered IPO in Figure 3b) that  
149 may be of great importance to the ongoing WAIS ice loss<sup>7</sup>. Comparing the PACE ensemble  
150 mean to the tropical response further illustrates the impact of the forced trend. The variability  
151 has not changed appreciably during the 20<sup>th</sup> century (Figure 3b), but absolute westerly wind  
152 anomalies that were rare have become commonplace (Figure 3a). Given the strong evidence  
153 for a positive relationship between zonal wind anomalies and CDW import, this implies that  
154 warm anomalies in the Amundsen Sea have become progressively more prevalent through  
155 the 20<sup>th</sup> century as a result of radiative forcing.

156

157 Radiative forcing has several sources, both anthropogenic (greenhouse gases, ozone,  
158 aerosols, land use) and natural (volcanoes, solar). The LENS ensemble mean represents the  
159 net effect of all sources, and additional simulations would be required to formally isolate the  
160 anthropogenic contribution. However, previous work has shown that forced trends in the  
161 southern sub-polar westerlies are dominated by anthropogenic influences<sup>33-35</sup>. In contrast,  
162 there is no conclusive evidence that Pacific variability has been significantly affected by  
163 anthropogenic forcing<sup>36,37</sup>. Therefore, the evidence suggests that the forced trend in PITT  
164 winds is primarily anthropogenic in origin, while the influence of the tropical Pacific is  
165 primarily natural.

166

167 **Implications for the West Antarctic Ice Sheet**

168 This analysis of the climate model ensembles offers a plausible narrative for the ongoing WAIS  
169 ice loss. i) In the 1920s, the WAIS was closer to balance with cooler Amundsen Sea conditions  
170 associated with mean easterly PITT winds. ii) Through the 20<sup>th</sup> century, the mean easterlies  
171 were progressively weakened by anthropogenic radiative forcing, causing tropically-forced  
172 decadal warm ocean anomalies to become more prevalent at the ice-sheet margin. iii)  
173 Episodes of particularly strong eastward wind anomalies, e.g. around 1940 (refs. <sup>28,29</sup>), created  
174 strong melting anomalies that caused ice streams to un-ground from seabed ridges,  
175 prompting progressive retreat as a result of ice and ocean feedbacks<sup>10,11</sup>. iv) As warm  
176 anomalies became more prevalent in recent decades, the ice-sheet imbalance was  
177 exacerbated, reaching the present-day rate.

178

179 Figure 5 illustrates this narrative by comparing PACE ensemble-mean winds to the  
180 glaciological evidence. Prominent eastward wind anomalies around 1940 and 1970 are  
181 consistent with the dates of initial and final ungrounding of Pine Island Glacier from a seabed  
182 ridge inferred from sediment records and remote sensing<sup>8,12</sup>. Since 1980, eastward wind  
183 anomalies have triggered accelerations in glacial discharge<sup>3</sup> that induced drawdown of inland  
184 ice<sup>4</sup>. These eastward anomalies reflect Pacific variability that is not at all unusual in the record  
185 (Figure 3b). However, when superimposed upon the anthropogenic trend this variability  
186 produces periods of absolute westerly winds that are sufficiently anomalous to account for  
187 much of the current ice loss.

188

189 This narrative proposes that present-day ice loss is driven by an anthropogenically-forced  
190 melting imbalance modulated by natural tropical variability and ice—ocean feedbacks. The  
191 WAIS lost mass during recent warm ocean anomalies, but did not gain mass during cool



192 anomalies<sup>3,4,6,38</sup>, an asymmetry that is consistent with both ice—ocean feedbacks and with  
193 the ice sheet being historically in balance with cooler ocean conditions. However, we caution  
194 that other narratives cannot yet be discounted, including those based solely on long-term  
195 natural variability in ice sheet dynamics and climate forcing (e.g. the IPO).

196

197 The unknown timing and magnitude of internal variability – other than that related to the  
198 tropical Pacific – adds considerable uncertainty to the actual trend in PITT winds over the 20<sup>th</sup>  
199 century. All PACE simulations are equally plausible, and the standard deviation of PACE trends  
200 is nearly half the mean trend (Table 1, Supplementary Figure S6). In addition, the centennial  
201 trends are much smaller than decadal internal variability. In observations and CESM  
202 simulations, the ~0.5 m/s variability has equivalent magnitude to ~100 years of the mean  
203 forced trends (Table 1, Figure 3). Decadal internal variability therefore dominates ice sheet  
204 and ocean variability during the modern observational era (since 1979), and will continue to  
205 dominate observations for decades to come.

206

207 While weaker than decadal variability on short timescales, on centennial timescales we  
208 suggest that the wind trend is sufficiently large to have influenced ice-sheet stability. Recent  
209 Pine Island Glacier ice-shelf melting anomalies of ~40 Gt/y are associated with PACE ensemble  
210 mean wind anomalies of ~1.5 m/s (Figure 5). If this ratio held for centennial trends, the PACE  
211 mean trend of ~0.7 m/s/century would induce a melting trend of ~20 Gt/y/century.  
212 Integrated over 100 years, this is half the magnitude of the decadal melting anomalies that  
213 affect ice-sheet mass balance (Figure 5). Furthermore, Pine Island Glacier discharge was ~80  
214 Gt/y in 1974 (ref. <sup>3</sup>). If half was accounted for by melting<sup>39</sup>, the integrated centennial trend  
215 would represent a 50% increase in melting over the 1974 rate. This simple argument supports

216 the importance of the wind trends, but the centennial relationship between winds and  
217 melting remains a topic of considerable uncertainty that requires much further research.

218

### 219 **Future projections**

220 The historical PITT wind trend continues through the 21<sup>st</sup> century for the high-emissions  
221 RCP8.5 scenario, with LENS and CMIP5 projecting a mean trend of ~0.4 m/s/century (Table 1;  
222 Figures 3 and 4c). This suggests that warmer Amundsen Sea conditions will become  
223 progressively more prevalent. By 2100 the mean westerly is comparable to 1 standard  
224 deviation of the internal variability, so the wind is reliably westerly (Table 1). The total 1920—  
225 2100 wind change is equivalent to ~2 standard deviations of the internal variability, so if the  
226 WAIS were close to balance with ocean conditions in the 1920s, this suggests substantial ice-  
227 sheet change by 2100.

228

229 As described above, radiative forcing impacts in this region are dominated by anthropogenic  
230 influences, primarily ozone depletion and greenhouse gases<sup>33-35</sup>. Thirty-year wind trends  
231 within the CESM centennial records (Supplementary Figure S7) show elevated trends centred  
232 on the 1980s and reduced trends centred on 2030 that represent the influence of ozone  
233 depletion and recovery. In the RCP8.5 scenario, the effect of ozone depletion causes only a  
234 temporary perturbation to the underlying trend, caused by greenhouse gases, that persists  
235 throughout the 20<sup>th</sup> and 21<sup>st</sup> centuries.

236

237 Of course, 21<sup>st</sup> century radiative forcing is not decided. Under RCP4.5, CMIP5 simulations  
238 project PITT wind trends that are not significantly different from zero (Table 1, Figures 3d and  
239 4c; Supplementary Figure S6) because ozone recovery fully compensates the weaker

240 greenhouse-gas forcing in this scenario<sup>40</sup>. The difference between CMIP5 RCP4.5 and RCP8.5  
241 wind trends is significant at the 95% confidence level (Supplementary Tables S2 and S3).  
242 Alternative evidence can be gained by comparing the LENS RCP8.5 projection to the CESM  
243 ‘medium ensemble’ (MENS; ref. <sup>41</sup>), a 15-member ensemble of RCP4.5 projections (Methods).  
244 The 2006-2080 MENS mean projected wind trend is lower than that of LENS, but unlike the  
245 CMIP5 results this difference is not statistically significant (Supplementary Tables S2 and S3).  
246  
247 The CMIP5 RCP4.5/8.5 comparison samples a range of model responses to radiative forcing,  
248 while the LENS/MENS comparison better characterises the role of internal variability, in a  
249 model with exceptionally low mean-state bias. Overall, these results suggest that weaker  
250 wind trends under RCP4.5 lead to Amundsen Sea ocean conditions frequently cooler than  
251 under RCP8.5. RCP4.5 and RCP8.5 scenarios differ in a specific sub-set of anthropogenic  
252 forcings (greenhouse gases, aerosols, land use), suggesting that policymakers have an  
253 opportunity to ‘weight the dice’ towards a lower future sea-level contribution from the WAIS.  
254 This conclusion relates to ocean changes induced by wind forcing, the mode of variability that  
255 has dominated observations<sup>5,6</sup>. The future contribution of additional warming mechanisms,  
256 such as a general warming of the CDW entering the Amundsen Sea, is highly uncertain<sup>42</sup>.  
257  
258 Owing to the unpredictable phasing of internal climate variability, there is significant variance  
259 in wind trends between ensemble members, with the one-standard-deviation range for LENS  
260 and MENS extending between no trend and twice the mean trend (Supplementary Figure S6).  
261 Internal variability is therefore of comparable importance to radiative forcing in determining  
262 the magnitude of PITT wind changes during the 21<sup>st</sup> century. In the CMIP5 ensembles, inter-  
263 model differences add further uncertainty to the future trajectory of PITT winds

264 (Supplementary Figure S6). To deliver meaningful projections of the WAIS over this period,  
265 ice sheet models will need to adopt an ensemble approach forced by multiple realisations of  
266 ocean melting.

267

#### 268 **Data Availability**

269 Sea ice concentration and drift data that support the findings of this study are available from  
270 the National Snow and Ice Data Center (<https://doi.org/10.5067/8GQ8LZQVLOVL> and  
271 <https://doi.org/10.5067/O57VAIT2AYYY> respectively). ERA-Interim reanalysis data are  
272 available from the European Centre for Medium-Range Weather Forecasts  
273 (<https://apps.ecmwf.int/datasets/data/interim-full-daily>). Extended Reconstructed Sea-  
274 surface Temperature data are available from the National Oceanic and Atmospheric  
275 Administration National Climatic Data Center ([https://www.ncdc.noaa.gov/data-  
276 access/marineocean-data/extended-reconstructed-sea-surface-temperature-ersst-v5](https://www.ncdc.noaa.gov/data-access/marineocean-data/extended-reconstructed-sea-surface-temperature-ersst-v5)).

277 Seabed data are available from the British Antarctic Survey  
278 (<https://secure.antarctica.ac.uk/data/bedmap2>). Climate indices are available from the  
279 National Oceanic and Atmospheric Administration Earth System Research Laboratory  
280 (<https://www.esrl.noaa.gov/psd/data/climateindices/list>). CMIP5 simulation data are  
281 available from the Centre for Environmental Data Analysis (<http://www.ceda.ac.uk>). CESM  
282 simulation data are available from the National Center for Atmospheric Research Climate  
283 Data Gateway (<https://www.earthsystemgrid.org>).

284

#### 285 **Code Availability**

286 The Matlab scripts used for the analyses described in this study can be obtained from the  
287 corresponding author upon reasonable request.

289 **References**

- 290 1 Shepherd, A. *et al.* Mass balance of the Antarctic Ice Sheet from 1992 to 2017. *Nature* **558**,  
291 219-222, doi:10.1038/s41586-018-0179-y (2018).
- 292 2 Shepherd, A., Wingham, D. & Rignot, E. Warm ocean is eroding West Antarctic Ice Sheet.  
293 *Geophys Res Lett* **31**, L23402, doi:10.1029/2004gl021106 (2004).
- 294 3 Mougnot, J., Rignot, E. & Scheuchl, B. Sustained increase in ice discharge from the Amundsen  
295 Sea Embayment, West Antarctica, from 1973 to 2013. *Geophys Res Lett* **41**, 1576-1584,  
296 doi:10.1002/2013gl059069 (2014).
- 297 4 Konrad, H. *et al.* Uneven onset and pace of ice-dynamical imbalance in the Amundsen Sea  
298 Embayment, West Antarctica. *Geophys Res Lett*, 910-918, doi:10.1002/2016GL070733 (2017).
- 299 5 Jenkins, A. *et al.* Decadal ocean forcing and Antarctic Ice Sheet response: Lessons from the  
300 Amundsen Sea. *Oceanography* **29**, 106-117, doi:10.5670/oceanog.2016.103 (2016).
- 301 6 Jenkins, A. *et al.* West Antarctic Ice Sheet retreat in the Amundsen Sea driven by decadal  
302 oceanic variability. *Nat Geosci* **11**, 733-738, doi:10.1038/s41561-018-0207-4 (2018).
- 303 7 Snow, K. *et al.* The Response of Ice Sheets to Climate Variability. *Geophys Res Lett* **44**, 11878-  
304 11885, doi:10.1002/2017gl075745 (2017).
- 305 8 Jenkins, A. *et al.* Observations beneath Pine Island Glacier in West Antarctica and implications  
306 for its retreat. *Nat Geosci* **3**, 468-472, doi:10.1038/Ngeo890 (2010).
- 307 9 Steig, E. J., Ding, Q., Battisti, D. S. & Jenkins, A. Tropical forcing of Circumpolar Deep Water  
308 Inflow and outlet glacier thinning in the Amundsen Sea Embayment, West Antarctica. *Annals*  
309 *of Glaciology* **53**, 19-28, doi:10.3189/2012AoG60A110 (2012).
- 310 10 De Rydt, J., Holland, P. R., Dutrieux, P. & Jenkins, A. Geometric and oceanographic controls on  
311 melting beneath Pine Island Glacier. *J Geophys Res-Oceans* **119**, 2420-2438,  
312 doi:10.1002/2013JC009513 (2014).
- 313 11 De Rydt, J. & Gudmundsson, G. H. Coupled ice shelf-ocean modeling and complex grounding  
314 line retreat from a seabed ridge. *Journal of Geophysical Research-Earth Surface* **121**, 865-880,  
315 doi:10.1002/2015jf003791 (2016).
- 316 12 Smith, J. A. *et al.* Sub-ice-shelf sediments record history of twentieth-century retreat of Pine  
317 Island Glacier. *Nature* **541**, 77-80, doi:10.1038/nature20136 (2016).
- 318 13 Jacobs, S. S., Hellmer, H. H. & Jenkins, A. Antarctic ice sheet melting in the Southeast Pacific.  
319 *Geophys Res Lett* **23**, 957-960 (1996).
- 320 14 Dutrieux, P. *et al.* Strong Sensitivity of Pine Island Ice-Shelf Melting to Climatic Variability.  
321 *Science* **343**, 174-178, doi:10.1126/science.1244341 (2014).
- 322 15 Thoma, M., Jenkins, A., Holland, D. & Jacobs, S. Modelling Circumpolar Deep Water intrusions  
323 on the Amundsen Sea continental shelf, Antarctica. *Geophys Res Lett* **35**, L18602,  
324 doi:10.1029/2008gl034939 (2008).
- 325 16 Kimura, S. *et al.* Oceanographic Controls on the Variability of Ice-Shelf Basal Melting and  
326 Circulation of Glacial Meltwater in the Amundsen Sea Embayment, Antarctica. *J Geophys Res-*  
327 *Oceans* **122**, 10131-10155, doi:10.1002/2017jc012926 (2017).
- 328 17 Webber, B. G. M., Heywood, K. J., Stevens, D. P. & Assmann, K. M. The Impact of Overturning  
329 and Horizontal Circulation in Pine Island Trough on Ice Shelf Melt in the Eastern Amundsen  
330 Sea. *Journal of Physical Oceanography* **49**, 63-83, doi:10.1175/Jpo-D-17-0213.1 (2019).
- 331 18 Assmann, K. M. *et al.* Variability of Circumpolar Deep Water transport onto the Amundsen Sea  
332 continental shelf through a shelf break trough. *J Geophys Res-Oceans* **118**, 6603-6620,  
333 doi:10.1002/2013jc008871 (2013).
- 334 19 Walker, D. P., Jenkins, A., Assmann, K. M., Shoosmith, D. R. & Brandon, M. A. Oceanographic  
335 observations at the shelf break of the Amundsen Sea, Antarctica. *J Geophys Res-Oceans* **118**,  
336 2906-2918, doi:10.1002/Jgrc.20212 (2013).

337 20 St-Laurent, P., Klinck, J. M. & Dinniman, M. S. Impact of local winter cooling on the melt of  
338 Pine Island Glacier, Antarctica. *J Geophys Res-Oceans* **120**, 6718-6732,  
339 doi:10.1002/2015JC010709 (2015).

340 21 Davis, P. E. D. *et al.* Variability in Basal Melting Beneath Pine Island Ice Shelf on Weekly to  
341 Monthly Timescales. *J Geophys Res-Oceans* **123**, 8655-8669, doi:10.1029/2018jc014464  
342 (2018).

343 22 Webber, B. G. M. *et al.* Mechanisms driving variability in the ocean forcing of Pine Island  
344 Glacier. *Nat Commun* **8**, 14507, doi:10.1038/ncomms14507 (2017).

345 23 Kim, T. W. *et al.* Is Ekman pumping responsible for the seasonal variation of warm Circumpolar  
346 Deep Water in the Amundsen Sea? *Continental Shelf Research* **132**, 38-48,  
347 doi:10.1016/j.csr.2016.09.005 (2017).

348 24 Raphael, M. N. *et al.* The Amundsen Sea Low: Variability, Change, and Impact on Antarctic  
349 Climate. *Bulletin of the American Meteorological Society* **97**, 111-121, doi:10.1175/Bams-D-  
350 14-00018.1 (2016).

351 25 Lachlan-Cope, T. & Connolley, W. Teleconnections between the tropical Pacific and the  
352 Amundsen-Bellinghausens sea: Role of the El Nino Southern Oscillation. *Journal of*  
353 *Geophysical Research-Atmospheres* **111**, D23101, doi:10.1029/2005jd006386 (2006).

354 26 Deser, C., Alexander, M. A., Xie, S. P. & Phillips, A. S. Sea Surface Temperature Variability:  
355 Patterns and Mechanisms. *Annual Review of Marine Science* **2**, 115-143, doi:10.1146/annurev-  
356 marine-120408-151453 (2010).

357 27 Schneider, D. P. & Deser, C. Tropically driven and externally forced patterns of Antarctic sea  
358 ice change: reconciling observed and modeled trends. *Climate Dynamics* **50**, 4599-4618,  
359 doi:10.1007/s00382-017-3893-5 (2018).

360 28 Steig, E. J. *et al.* Recent climate and ice-sheet changes in West Antarctica compared with the  
361 past 2,000 years. *Nat Geosci* **6**, 372-375, doi:10.1038/Ngeo1778 (2013).

362 29 Schneider, D. P. & Steig, E. J. Ice cores record significant 1940s Antarctic warmth related to  
363 tropical climate variability. *Proceedings of the National Academy of Sciences of the United*  
364 *States of America* **105**, 12154-12158, doi:10.1073/pnas.0803627105 (2008).

365 30 Kay, J. E. *et al.* The Community Earth System Model (CESM) Large Ensemble Project: A  
366 Community Resource for Studying Climate Change in the Presence of Internal Climate  
367 Variability. *Bulletin of the American Meteorological Society* **96**, 1333-1349, doi:10.1175/Bams-  
368 D-13-00255.1 (2015).

369 31 Bracegirdle, T. J., Turner, J., Hosking, J. S. & Phillips, T. Sources of uncertainty in projections of  
370 21st century westerly wind changes over the Amundsen Sea, West Antarctica, in CMIP5  
371 climate models. *Climate Dynamics* **43**, 2093-2104, doi:10.1007/s00382-013-2032-1 (2014).

372 32 Harvey, B. J., Shaffrey, L. C. & Woollings, T. J. Equator-to-pole temperature differences and  
373 the extra-tropical storm track responses of the CMIP5 climate models. *Climate Dynamics* **43**,  
374 1171-1182, doi:10.1007/s00382-013-1883-9 (2014).

375 33 Arblaster, J. M. & Meehl, G. A. Contributions of external forcings to southern annular mode  
376 trends. *J Climate* **19**, 2896-2905, doi:10.1175/Jcli3774.1 (2006).

377 34 Schneider, D. P., Deser, C. & Fan, T. T. Comparing the Impacts of Tropical SST Variability and  
378 Polar Stratospheric Ozone Loss on the Southern Ocean Westerly Winds. *J Climate* **28**, 9350-  
379 9372, doi:10.1175/Jcli-D-15-0090.1 (2015).

380 35 Gillett, N. P., Fyfe, J. C. & Parker, D. E. Attribution of observed sea level pressure trends to  
381 greenhouse gas, aerosol, and ozone changes. *Geophys Res Lett* **40**, 2302-2306,  
382 doi:10.1002/grl.50500 (2013).

383 36 Yeh, S. W. *et al.* ENSO Atmospheric Teleconnections and Their Response to Greenhouse Gas  
384 Forcing. *Rev Geophys* **56**, 185-206, doi:10.1002/2017rg000568 (2018).

385 37 Cai, W. J. *et al.* ENSO and greenhouse warming. *Nat Clim Change* **5**, 849-859,  
386 doi:10.1038/Nclimate2743 (2015).

387 38 Christianson, K. *et al.* Sensitivity of Pine Island Glacier to observed ocean forcing. *Geophys Res*  
388 *Lett* **43**, 10817-10825, doi:10.1002/2016gl070500 (2016).

389 39 Rignot, E., Jacobs, S., Mouginot, J. & Scheuchl, B. Ice-Shelf Melting Around Antarctica. *Science*  
390 **341**, 266-270, doi:10.1126/science.1235798 (2013).

391 40 Barnes, E. A., Barnes, N. W. & Polvani, L. M. Delayed Southern Hemisphere Climate Change  
392 Induced by Stratospheric Ozone Recovery, as Projected by the CMIP5 Models. *J Climate* **27**,  
393 852-867, doi:10.1175/Jcli-D-13-00246.1 (2014).

394 41 Sanderson, B. M., Oleson, K. W., Strand, W. G., Lehner, F. & O'Neill, B. C. A new ensemble of  
395 GCM simulations to assess avoided impacts in a climate mitigation scenario. *Climatic Change*  
396 **146**, 303-318, doi:10.1007/s10584-015-1567-z (2018).

397 42 Little, C. M. & Urban, N. M. CMIP5 temperature biases and 21st century warming around the  
398 Antarctic coast. *Annals of Glaciology* **57**, 69-78, doi:10.1017/aog.2016.25 (2016).

399 43 Cavalieri, D. J., Parkinson, C. L., Gloersen, P. & Zwally, H. J. Sea Ice Concentrations from  
400 Nimbus-7 SMMR and DMSP SSM/I-SSMIS Passive Microwave Data, Version 1. 1992-2016.  
401 (National Snow and Ice Data Center, Boulder, Colorado, USA, 1996).

402 44 Tschudi, M., Fowler, C., Maslanik, J., Stewart, J. S. & Meier, W. Polar Pathfinder Daily 25 km  
403 EASE-Grid Sea Ice Motion Vectors, Version 3. 1992-2016. (National Snow and Ice Data  
404 Center, Boulder, Colorado, USA., 2016).

405 45 Dee, D. P. *et al.* The ERA-Interim reanalysis: configuration and performance of the data  
406 assimilation system. *Quarterly Journal of the Royal Meteorological Society* **137**, 553-597,  
407 doi:10.1002/Qj.828 (2011).

408 46 Fretwell, P. *et al.* Bedmap2: improved ice bed, surface and thickness datasets for Antarctica.  
409 *The Cryosphere* **7**, 375-393, doi:10.5194/tc-7-375-2013 (2013).

410 47 Huang, B. *et al.* NOAA Extended Reconstructed Sea Surface Temperature (ERSST). Version 5.  
411 1854-2016. (NOAA National Centers for Environmental Information, 2017).

412 48 Crosby, D. S., Breaker, L. C. & Gemmill, W. H. A Proposed Definition for Vector Correlation in  
413 Geophysics - Theory and Application. *Journal of Atmospheric and Oceanic Technology* **10**, 355-  
414 367 (1993).

415 49 Kim, C. S. *et al.* Variability of the Antarctic Coastal Current in the Amundsen Sea. *Estuarine*  
416 *Coastal and Shelf Science* **181**, 123-133, doi:10.1016/j.ecss.2016.08.004 (2016).

417 50 Mazur, A. K., Wåhlin, A. K. & Krezel, A. An object-based SAR image iceberg detection algorithm  
418 applied to the Amundsen Sea. *Remote Sensing of Environment* **189**, 67-83,  
419 doi:10.1016/j.rse.2016.11.013 (2017).

420 51 Zhang, Y., Wallace, J. M. & Battisti, D. S. ENSO-like interdecadal variability: 1900-93. *J Climate*  
421 **10**, 1004-1020, doi:10.1175/1520-0442(1997)010<1004:Eliv>2.0.Co;2 (1997).

422 52 Power, S., Casey, T., Folland, C., Colman, A. & Mehta, V. Inter-decadal modulation of the  
423 impact of ENSO on Australia. *Climate Dynamics* **15**, 319-324, doi:10.1007/s003820050284  
424 (1999).

425 53 Newman, M. *et al.* The Pacific Decadal Oscillation, Revisited. *J Climate* **29**, 4399-4427,  
426 doi:10.1175/Jcli-D-15-0508.1 (2016).

427 54 Henley, B. J. *et al.* A Tripole Index for the Interdecadal Pacific Oscillation. *Climate Dynamics*  
428 **45**, 3077-3090, doi:10.1007/s00382-015-2525-1 (2015).

429 55 Bretherton, C. S., Widmann, M., Dymnikov, V. P., Wallace, J. M. & Blade, I. The effective  
430 number of spatial degrees of freedom of a time-varying field. *J Climate* **12**, 1990-2009,  
431 doi:10.1175/1520-0442(1999)012<1990:Tenosd>2.0.Co;2 (1999).

432 56 Deser, C., Guo, R. X. & Lehner, F. The relative contributions of tropical Pacific sea surface  
433 temperatures and atmospheric internal variability to the recent global warming hiatus.  
434 *Geophys Res Lett* **44**, 7945-7954, doi:10.1002/2017gl074273 (2017).

435 57 Kosaka, Y. & Xie, S. P. Recent global-warming hiatus tied to equatorial Pacific surface cooling.  
436 *Nature* **501**, 403-407, doi:10.1038/nature12534 (2013).

437 58 Kosaka, Y. & Xie, S. P. The tropical Pacific as a key pacemaker of the variable rates of global  
438 warming. *Nat Geosci* **9**, 669-673, doi:10.1038/Ngeo2770 (2016).

439

#### 440 **Acknowledgements**

441 We are grateful to the originators of the many open-access datasets synthesised in this study,  
442 including remotely-sensed sea ice data, atmospheric reanalysis model results, sea-surface  
443 temperature and bathymetry observations, derived climate indices, and many climate model  
444 simulations. PD was supported by NSF awards 1643285 and 1644159. EJS was supported by  
445 NSF award 1602435.

446

#### 447 **Author Contributions**

448 PH conceived the study and led the data processing. TB processed the CMIP5 model results.  
449 All authors discussed the results and implications and collaborated on writing the manuscript  
450 at all stages.

451

452 **The authors declare no competing interests.**

453

#### 454 **Corresponding Author**

455 Correspondence to P. Holland (p.holland@bas.ac.uk)

456

#### 457 **Methods**

##### 458 **Observational datasets**

459 The total surface stress formulae employ daily ice concentration<sup>43</sup> and drift<sup>44</sup> data derived  
460 from passive microwave satellite data, and surface winds from the European Centre for



461 Medium-Range Weather Forecasts ERA-Interim reanalysis<sup>45</sup>. The results are set in context  
462 using the Bedmap2 seabed dataset<sup>46</sup>. The stress calculation is detailed below.

463

464 The variability of 10-m zonal winds and surface stresses in the Amundsen Sea are considered  
465 over a PITT box extending from 115°-102° W, 71.8°-70.2° S (Figure 1). This box is focussed  
466 upon the shelf-break mouths of the troughs feeding Pine Island and Thwaites glaciers, and is  
467 therefore both further south and smaller than that used by other authors<sup>5,6,9,14,15,31</sup>. The box  
468 used by these previous authors was chosen to reflect the coarser resolution of an earlier  
469 reanalysis dataset<sup>15</sup>. These PITT winds are set in their wider context using global SST data from  
470 the Extended Reconstructed SST (ERSST) v5 dataset<sup>47</sup>, and global SLP from ERA-Interim.  
471 Throughout the paper, the term ‘eastward’ is used to refer to wind anomalies oriented in the  
472 eastward direction, while the term ‘westerly’ is used to refer to a wind that is actually blowing  
473 from west to east in absolute terms.

474

#### 475 **Calculation of surface stresses**

476 The ‘total’ surface stress ( $\boldsymbol{\tau}$ ) is calculated simply as the sum of air—ocean ( $\boldsymbol{\tau}_a$ ) and ice—ocean  
477 ( $\boldsymbol{\tau}_i$ ) stresses, weighted by ice concentration ( $C$ ):

$$478 \quad \boldsymbol{\tau} = (1 - C)\boldsymbol{\tau}_a + C\boldsymbol{\tau}_i.$$

479 The individual stresses are represented as

$$480 \quad \boldsymbol{\tau}_a = \rho_a c_a |\mathbf{u}_a| \mathbf{u}_a$$

$$481 \quad \boldsymbol{\tau}_i = \rho_o c_o |\mathbf{u}_i| \mathbf{u}_i$$

482 where  $\mathbf{u}_a$  is the 10-m wind vector,  $\mathbf{u}_i$  is the observed ice drift vector,  $\rho_a=1.3 \text{ kg/m}^3$  and  $\rho_o=1030$   
483  $\text{kg/m}^3$  are air and ocean densities, and  $c_a=0.001$  and  $c_o=0.006$  are air and ocean drag  
484 coefficients.

485

486 This formulation is perhaps the simplest conceivable. There are many alterations that could  
487 be adopted<sup>23</sup>, such as including the ocean surface current, adopting an air-ocean stress  
488 formulation that accounts for sea state, or attempting to represent spatial and temporal  
489 variation in drag coefficients. These alternatives are not pursued because their requirement  
490 for additional unknown quantities implies they may not lead to a more realistic stress. In  
491 particular, including ocean currents in the stress calculation could radically alter the results<sup>16</sup>,  
492 but suitable current observations are not available. Our approach should be regarded as a  
493 simple first attempt to examine nominal total stresses in order to build understanding of the  
494 role of sea ice.

495

496 Ekman pumping by the total and wind-only stresses are calculated according to

$$497 \quad w\mathbf{k} = \frac{\nabla \times \boldsymbol{\tau}}{\rho_o f}$$

$$498 \quad w_a\mathbf{k} = \frac{\nabla \times \boldsymbol{\tau}_a}{\rho_o f}$$

499 where  $\mathbf{k}$  is the vertical unit vector and  $f=-1.4\times 10^{-4} \text{ s}^{-1}$  is the Coriolis parameter.

500

501 The above formulae employ daily ice concentration and drift data and reanalysis model winds.  
502 All datasets are used for 1992—2016, the period during which consistent passive microwave  
503 data are available, and are binned/interpolated to a 25 km resolution polar stereographic  
504 grid, upon which stresses are calculated. The stresses are smoothed spatially with a 3×3 grid  
505 cell mean to remove gridding artefacts manifested in the Ekman pumping fields. The vector  
506 correlation between total and wind-only stresses is calculated according to a technique that  
507 measures covariance in both magnitude and direction<sup>48</sup>.

508

509 Anomalies in the wind-only stress and total stress have a complex relationship on-shelf  
510 (Supplementary Figure S1). Their correlation drops near coasts because the ice strength  
511 resists convergence and shear. However, there are also significant polynyas on-shelf, where  
512 mobile ice permits a higher stress<sup>23,49</sup> that is better correlated to winds. The largest is the  
513 Amundsen Sea Polynya, which forms in the lee of icebergs grounded on a ridge north of Bear  
514 Island<sup>50</sup>. Shearing of mobile polynya ice against pack ice to the north-east creates Ekman  
515 upwelling<sup>23,49</sup>. Similar features occur west of Siple Island and Grant Island, which also host  
516 grounded icebergs<sup>50</sup>. Accounting for sea ice strongly affects the Ekman pumping. Ekman  
517 pumping is generally weak, with interannual variability of only ~5 m/y, suggesting that it  
518 cannot account for the large variations of CDW layer thickness that govern melting<sup>6,14</sup>.  
519 Therefore, we focus upon variations in CDW import to the shelf driven directly by zonal stress  
520 anomalies at the shelf break<sup>5,18,19</sup>. Accounting for sea ice has little effect on zonal stress  
521 anomalies at the shelf break, so zonal winds are used as a proxy for zonal stress at the shelf  
522 break throughout the study.

523

#### 524 **Climate indices**

525 The linkage between Amundsen Sea winds and a broad range of climatic indices  
526 (<https://www.esrl.noaa.gov/psd/data/climateindices/list/>) are considered, but the SOI and  
527 IPO are particularly emphasised. All measures of ENSO and Pacific decadal variability are  
528 correlated so the choice is not of crucial importance; the two chosen indices are most highly  
529 correlated with PITT winds (Supplementary Figure S4).

530

531 The SOI (<http://www.cpc.ncep.noaa.gov/data/indices/soi>) is a measure of ENSO variability. It  
532 is derived from the sea-level pressure difference between Tahiti and Australia (Figure 3c), a  
533 measure of anomalous atmospheric convection over the tropical Pacific. The SOI is positive  
534 during La Niña conditions, so we consider –SOI in order to align the index with the other  
535 measures considered.

536

537 The tripole IPO index (<https://www.esrl.noaa.gov/psd/data/timeseries/IPOTPI/>) is a measure  
538 of decadal variability in the Pacific climate system. This variability resembles ENSO but acts  
539 on longer timescales, features a different spatial pattern, and involves a variety of climate  
540 processes<sup>51-53</sup>. Pacific decadal variability has been characterised in several ways, for example  
541 as the second principal component (PC2) of monthly Pacific SST anomalies after a 13-year  
542 low-pass filter (PC1 being global warming)<sup>54</sup>. The ‘tripole’ index employed here uses the SST  
543 anomaly between three areas of the tropical and subtropical Pacific (Figure 2d) to represent  
544 the pattern of the associated Empirical Orthogonal Function and thus can be used to  
545 approximate the PC<sup>54</sup>. This index can be considered monthly (unfiltered), or subjected to a  
546 13-year low-pass filter to recover decadal variability similar to that of the original PC. The  
547 unfiltered index represents the monthly variability that underlies the decadal variability.

548

#### 549 **Significance of time series correlations**

550 Several figures involve the calculation of correlations between timeseries. These correlations  
551 are calculated on detrended time series at zero lag, after the application of a 2-year running  
552 mean. Owing to the use of a 2-year running mean throughout this study, the effective number  
553 of degrees of freedom in these correlations is relatively small for the 1979-2017 period used  
554 in Figures 2, S3, and S4. The effective sample size was analysed, accounting for

555 autocorrelation<sup>55</sup>, and in all cases was found to be very close to  $Y/2$ , where  $Y$  is the number  
556 of years in the record. This is the expected result for timeseries subjected to a 2-year running  
557 mean that have negligible autocorrelation on timescales longer than 2 years. Therefore, we  
558 derive the statistical significance of the correlations using a 2-sided t-test with  $Y/2$  as the  
559 degrees of freedom.

560

### 561 **Climate model simulations**

562 We examine Amundsen Sea winds in climate model simulations, including the Coupled Model  
563 Intercomparison Project 5 (CMIP5) archive<sup>31</sup>, the Community Earth System Model (CESM)  
564 Large Ensemble (LENS)<sup>30</sup>, CESM Medium Ensemble (MENS)<sup>41</sup>, and CESM tropical Pacific  
565 ‘pacemaker’ simulations (PACE)<sup>56</sup>. CMIP5 data were obtained from the Centre for  
566 Environmental Data Analysis (<http://www.ceda.ac.uk/>), while the CESM simulations were  
567 obtained from the National Center for Atmospheric Research Climate Data Gateway  
568 (<https://www.earthsystemgrid.org/>). The ensembles used are summarised in Supplementary  
569 Table S1.

570

571 For the ensemble of CMIP5 simulations, the models and processing follow an earlier study<sup>31</sup>.  
572 Data were assessed from ‘historical’ forcing simulations from 1920–2005 and future  
573 projections using (Representative Concentration Pathway) RCP4.5 and RCP8.5 from 2006–  
574 2100. We include only the first simulation from each different model to ensure the models  
575 are weighted equally, totalling 30 (31) realisations of RCP4.5 (RCP8.5). The historical ensemble  
576 includes the 31 simulations that continue to the RCP8.5 projection. RCP4.5 features a  
577 radiative forcing that stabilises in 2100, while RCP8.5 represents a continually increasing  
578 forcing. In both scenarios, stratospheric ozone recovers to near pre-ozone hole levels by 2100.

579 For each scenario, the spread between ensemble members reflects a combination of both  
580 model uncertainty and internal climate variability. By comparing the projected trends in the  
581 two ensembles, we are able to determine the influence of future radiative forcing upon PITT  
582 winds.

583

584 The LENS ensemble comprises 40 simulations of the CESM1.1 coupled climate model, in which  
585 the atmosphere, sea ice, and ocean models have a resolution of  $\sim 1^\circ$  (ref. <sup>30</sup>). Each simulation  
586 represents the period 1920-2100, using 'historical' forcings until 2005 and RCP8.5 afterwards.  
587 The CESM and its direct ancestors are not included in the CMIP5 ensemble analysed here. The  
588 only difference between LENS ensemble members is a random machine-precision ( $10^{-14}$  °C)  
589 perturbation to the initial atmospheric temperature, which rapidly grows in the chaotic  
590 climate system. Since the model physics are identical in all simulations, the spread between  
591 ensemble members represents only the influence of random internal climate variability.

592

593 The MENS ensemble comprises 15 simulations of the same model as LENS. MENS simulations  
594 are identical to LENS in every way apart from the projected radiative forcing, which follows  
595 RCP4.5 instead of RCP8.5. MENS simulations branch from the first 15 members of LENS in  
596 2006, running until 2080. Comparing MENS and LENS reveals the influence of radiative forcing  
597 scenario upon PITT winds within the CESM model. This offers additional information to the  
598 CMIP5 comparison because the CESM model has exceptionally low bias, and the difference  
599 between ensemble members is caused only by internal climate variability, free from the  
600 influence of model structural difference.

601

602 One complication is that MENS simulations only run until 2080, rather than 2100 in the other  
603 ensembles. Supplementary Tables S2 and S3 report LENS ensemble metrics for both the  
604 period to 2080 and 2100, for ease of comparison to MENS. The LENS trends are larger over  
605 the longer period, and their difference to MENS more significant. However, we have no way  
606 of knowing how MENS would evolve after 2080, so in the main paper we rely upon the 2006-  
607 2080 trends, for which the difference between LENS and MENS ensembles is not statistically  
608 significant (Supplementary Table S3). This is partly a result of the relatively small size of MENS.

609

610 The PACE ensemble comprises 20 historical simulations (1920—2013) of the CESM1.1 model,  
611 in which eastern tropical Pacific SSTs are constrained to follow their observed history<sup>56</sup>. The  
612 restoring imposes SST anomalies in the region between 15°S-15°N and 180°W to the coast of  
613 the Americas, plus a restoring ramp-down region of 5° to the north, south, and west<sup>57</sup>. The  
614 restoring replaces model temporal SST anomalies with observed temporal SST anomalies.  
615 Therefore, to a first approximation, the restoring does not alter any mean-state bias in the  
616 climate model. The non-conservation of heat induced by the restoring is typically smaller than  
617 both the top-of-atmosphere radiation imbalance, and its model ensemble spread<sup>58</sup>. PACE  
618 simulations use historical forcings for 1920—2005 and RCP8.5 forcings for 2006—2013. The  
619 models used in the LENS and PACE ensembles are structurally identical. The forcing of the two  
620 ensembles is also identical apart from the representation of ozone depletion, which is derived  
621 from different datasets in the two ensembles<sup>27</sup>. This difference in ozone forcing has some  
622 effect on stratospheric temperatures, but no discernible effect upon the surface winds that  
623 are the focus of this study<sup>34</sup>. This is evident from the absence of any noticeable signature of  
624 ozone depletion in the tropical response (the mean difference between PACE and LENS; see  
625 below) in Figure 3b. Since all PACE ensemble members have identical model structure and are

626 constrained to follow the observed history of eastern and central tropical Pacific SST  
627 anomalies, the spread between PACE ensemble members represents internal climate  
628 variability that is associated with SSTs outside this region.

629

### 630 **Interpretation of climate model results**

631 The real climate trajectory combines the effects of a single realisation of random internal  
632 climate variability with a response to external forcings (greenhouse gases, ozone, aerosols,  
633 land use, volcanoes, solar). Therefore it should be most comparable to an individual member  
634 from our ensembles. However, model representations of the climate system are imperfect.  
635 The value of our model ensembles is therefore in helping to distinguish the effects of forcing,  
636 internal variability, and model uncertainty.

637

638 The CMIP5 ensemble spread represents both model uncertainty and internal climate  
639 variability. The LENS and MENS ensemble spread represents only internal variability. The  
640 PACE ensemble spread represents only internal variability associated with regions outside the  
641 eastern tropical Pacific. The CMIP5, LENS, and MENS ensemble means are derived by  
642 averaging over multiple realisations of random internal climate variability, and therefore  
643 represent estimates of the climate response to external forcings. These estimates differ in  
644 that the CMIP5 ensemble mean includes model uncertainty in the forced response, while the  
645 LENS and MENS ensemble means more accurately estimate the forced response of a single  
646 model. The PACE ensemble mean estimates the combined effect of the forced response and  
647 the real variability associated with the observed trajectory of tropical Pacific SSTs.

648



649 The influence of Pacific variability on the historical PITT wind trend can be deduced from  
650 differences between PACE and LENS. There are significant summer and autumn trends in both  
651 ensembles, while only PACE has trends in winter and spring (Supplementary Table S2). As a  
652 result, the PACE annual trend is higher than that of LENS (Table 1, Supplementary Figure S6).  
653 This difference between PACE and LENS mean trends is significant at the 95% confidence level  
654 for annual trends and for winter and spring (Supplementary Table S3), suggesting that Pacific  
655 variability made a small but detectable enhancement to the radiatively forced trend during  
656 the 20<sup>th</sup> century.

657

658 Since the PACE and LENS ensembles use the same model, their response to external forcing  
659 should in principle be the same. Therefore, we define the LENS ensemble mean as  
660 representing the ‘forced response’ in both the LENS and PACE ensembles. We may then  
661 subtract the LENS ensemble mean from the PACE ensemble mean to isolate the ‘tropical  
662 response’<sup>27</sup>. This tropical response is an estimate of the unforced variability in the climate  
663 system that is associated with tropical Pacific SSTs. The crucial advantage in this approach is  
664 that it allows us to consistently compare the magnitude of climate responses (e.g. PITT winds)  
665 to external forcing (forced response) and tropical Pacific variability (tropical response).  
666 Tropical response winds closely follow the unfiltered IPO index (Figure 3b), clarifying the  
667 causality of the linkage. When tropical Pacific SSTs are prescribed, PITT winds covary with the  
668 whole-Pacific SST pattern that results (hence they vary with the unfiltered IPO index). Since  
669 the unfiltered IPO index represents variability that underlies decadal variability upon filtering,  
670 this implies that PITT winds follow the decadal variability of the IPO.

671

672 There are several caveats to the interpretation of the tropical response. First, the approach  
673 assumes that the forced and tropical responses are linearly separable, thus neglecting the  
674 role of external forcing upon tropical variability. Second, the LENS and PACE ensembles have  
675 different ozone forcing, which could contaminate the tropical response, though the impact of  
676 this difference on surface winds is known to be small<sup>34</sup>, and our results support this (Figure  
677 3b). Third, the forced response in the LENS and PACE ensembles may actually differ, since the  
678 restoring in the latter alters the SST trend within the restoring region<sup>58</sup>. Ultimately, however,  
679 the results of many studies show that the ‘tropical response’ concept realistically and usefully  
680 depicts the influence of tropical Pacific variability<sup>27</sup>.

681

#### 682 **Amundsen Sea ice-shelf melting timeseries**

683 Figure 5 shows a timeseries of ice-shelf melt rates derived from ocean observations near Pine  
684 Island Glacier (PIG)<sup>5,14</sup> and Dotson Ice Shelf (DIS)<sup>6</sup>. Including both ice shelves offers improved  
685 temporal coverage, since most oceanographic surveys sampled only one of the two ice fronts.  
686 While the two ice shelves occupy distinct seabed troughs, and differ in the details of their  
687 geometry and oceanographic forcing, the phasing of their interannual variability is coherent  
688 and thought to be driven by common shelf-break wind forcing<sup>5,6,14,16</sup>. The derivation of melt  
689 rates for each ice shelf is fully documented in the original papers<sup>6,14</sup>, and only their  
690 combination requires further explanation here.

691

692 To display a consistent time series, we scale the DIS melt rates to produce an approximate  
693 PIG-equivalent melt rate. The scaling is derived from three years which have melt rates for  
694 both cavities (2009, 2012, 2014), which fortuitously includes the maximum and minimum

695 observed melt rates for both cavities. PIG-equivalent DIS melt rates are derived by regressing  
696 PIG melt rates against DIS melt rates for these three years, yielding

697 
$$m_{PIGeq} = 23.9 + 0.54 m_{DIS},$$

698 where all values are in Gt/y. These PIG-equivalent DIS melt rates are then combined with  
699 unscaled PIG melt rates to create the melt timeseries. The mean of the two melt values is  
700 used for years where both cavities were sampled. The combination of the two cavities is based  
701 upon only three common years and is therefore offered only for illustrative purposes.  
702 Nevertheless, the combined time series offers a credible account of decadal variability in the  
703 Amundsen Sea that is consistent with the independent ERA-Interim winds (Figure 5).

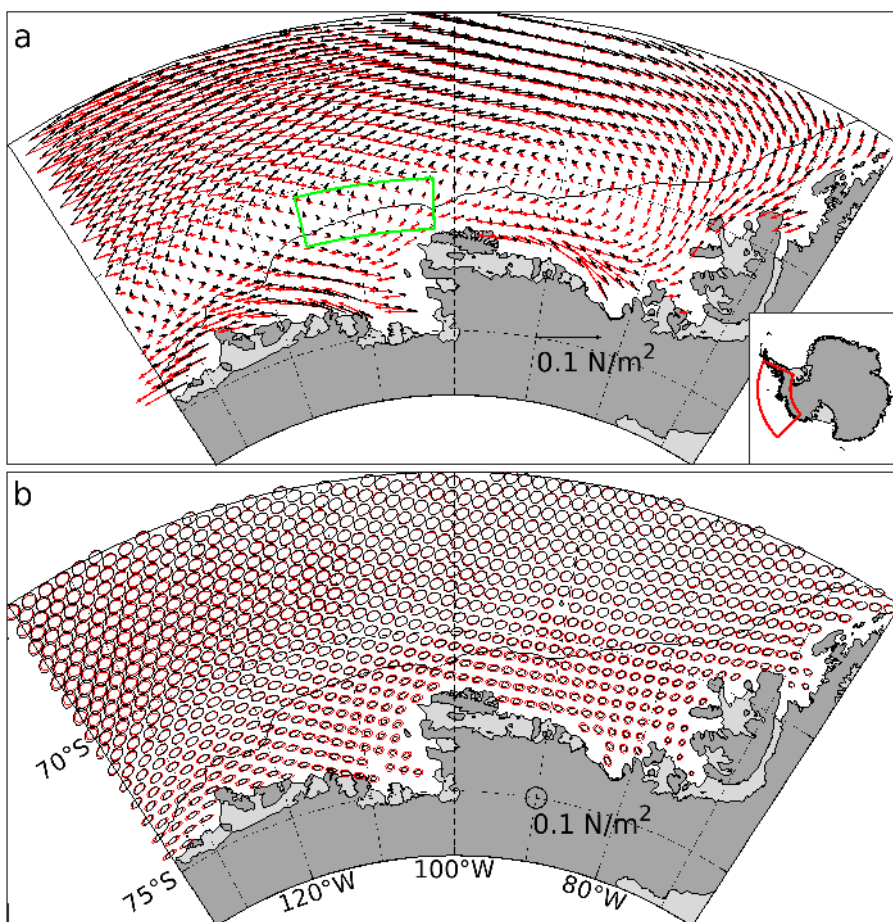
704 **Tables**

	Wind variability standard deviation of residuals from linear trends m/s	Wind trend mean $\pm$ 1 s.d. of trends in ensemble members m/s/century
ERA-Interim 1979-2016	0.49	0.04
PACE historical 1920-2005	0.54	<b>0.69 <math>\pm</math> 0.27</b>
LENS historical 1920-2005	0.60	<b>0.45 <math>\pm</math> 0.35</b>
CMIP5 historical 1920-2005	0.49	0.05 $\pm$ 0.36
MENS RCP4.5 2006-2080	0.59	<b>0.24 <math>\pm</math> 0.27</b>
LENS RCP8.5 2006-2100	0.58	<b>0.38 <math>\pm</math> 0.29</b>
CMIP5 RCP4.5 2006-2100	0.48	0.13 $\pm$ 0.47
CMIP5 RCP8.5 2006-2100	0.48	<b>0.36 <math>\pm</math> 0.48</b>

705 **Table 1: Variability and trends in Amundsen Sea winds in the climate model ensembles.**

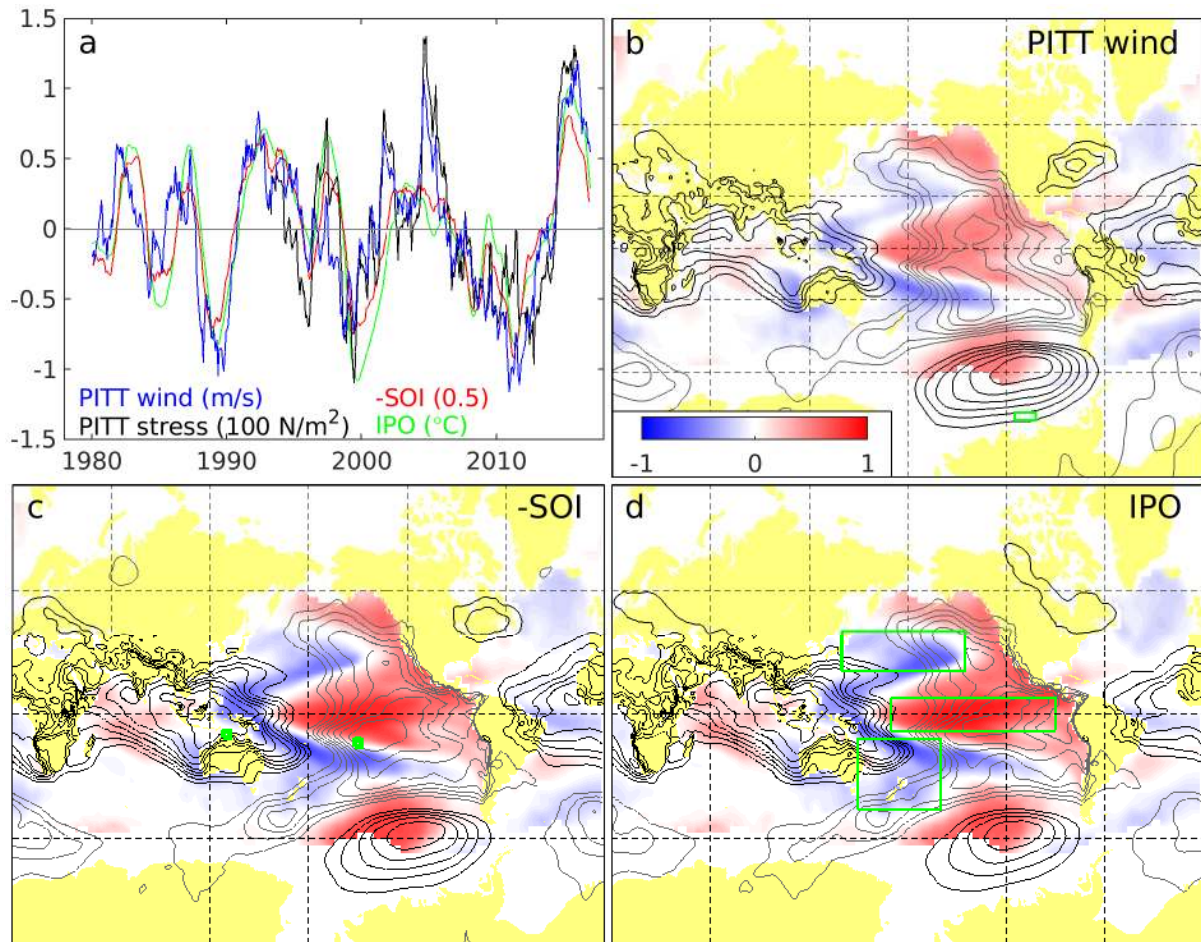
706 Variability in PITT winds is characterised by the standard deviation of residuals from the linear  
707 trends in all ensemble members. Note the timeseries have a 2-year running mean applied.  
708 Trends are characterised by the mean and standard deviation of the distribution of linear  
709 trends in the ensemble members. Mean trends in bold are significantly different from zero at  
710 the 99% confidence level under a one-sample t-test. CMIP5 historical and CMIP5 RCP4.5  
711 projected mean trends are not significant at the 90% level.

712 **Figures**



713

714 **Figure 1: Total surface stress and wind-only stress on the Amundsen Sea.** a) Mean 1992-  
715 2016 total stress (accounting for sea ice; black) and wind-only stress (red). b) Variance ellipses  
716 for monthly total and wind-only stress anomalies from seasonal climatology, aligned in the  
717 direction of maximum variance and scaled to 1 standard deviation. Vectors and ellipses are  
718 shown every second data point. The 1000 m depth contour at the shelf break is also shown.  
719 The green box shows the area of the Pine Island and Thwaites Troughs (PITT) at the shelf  
720 break, over which timeseries are calculated.



721

722 **Figure 2: Linkages between Amundsen Sea winds and global sea-surface temperature and**

723 **sea-level pressure.** a) Time series of zonal wind and zonal total stress over the PITT box, the

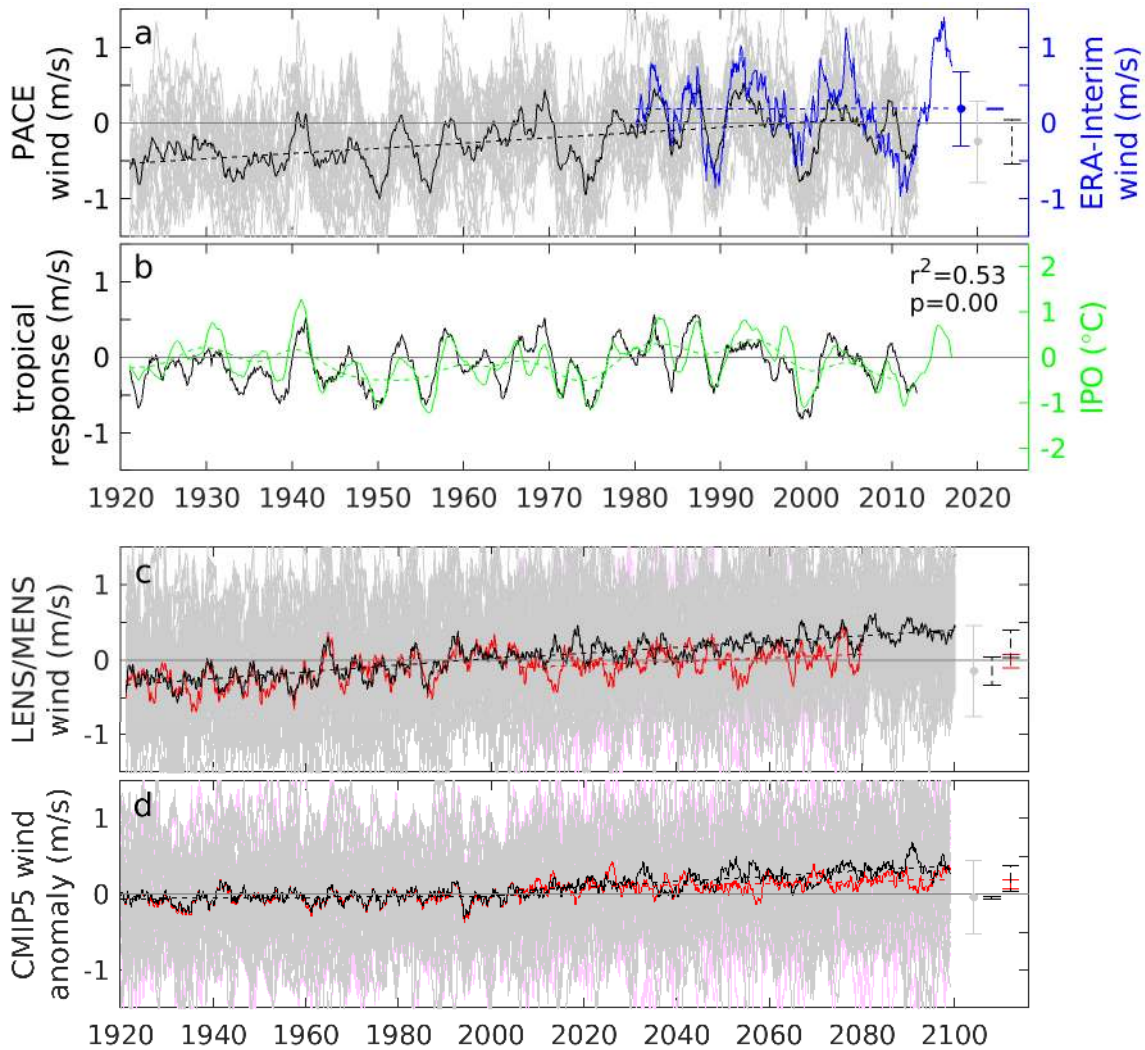
724 Southern Oscillation Index, and the Interdecadal Pacific Oscillation. The legend shows the

725 scaling for each timeseries. b-d) correlation maps of SST (colour) and SLP (contours) to PITT

726 winds and SOI and IPO indices. The maps show  $r^2$  multiplied by the sign of the relationship.

727 SLP correlation contours have a spacing of 0.1, with black positive, grey negative, and the zero

728 contour omitted. The area of each index is shown in green.



729

730 **Figure 3: Amundsen Sea winds within climate model ensembles.** a) Zonal winds over the  
 731 PITT box from ERA-Interim (blue), PACE simulations (grey), PACE ensemble mean (black) and  
 732 mean trend (dashed). b) ‘tropical response’ wind (black) and IPO index before (green) and  
 733 after (dashed) 13-year low-pass filter. c) Historical and projection simulations of LENS  
 734 (grey/black; RCP8.5) and MENS (pink/red; RCP4.5) ensembles. d) CMIP5 ensemble, including  
 735 RCP8.5 (grey/black) and RCP4.5 (pink/red). Error bars show the standard deviation of wind  
 736 anomalies (solid) and magnitude of historical and projected trends (dashed). CMIP5 models  
 737 contain large biases, so panel d shows anomalies from the 1979–2017 mean.



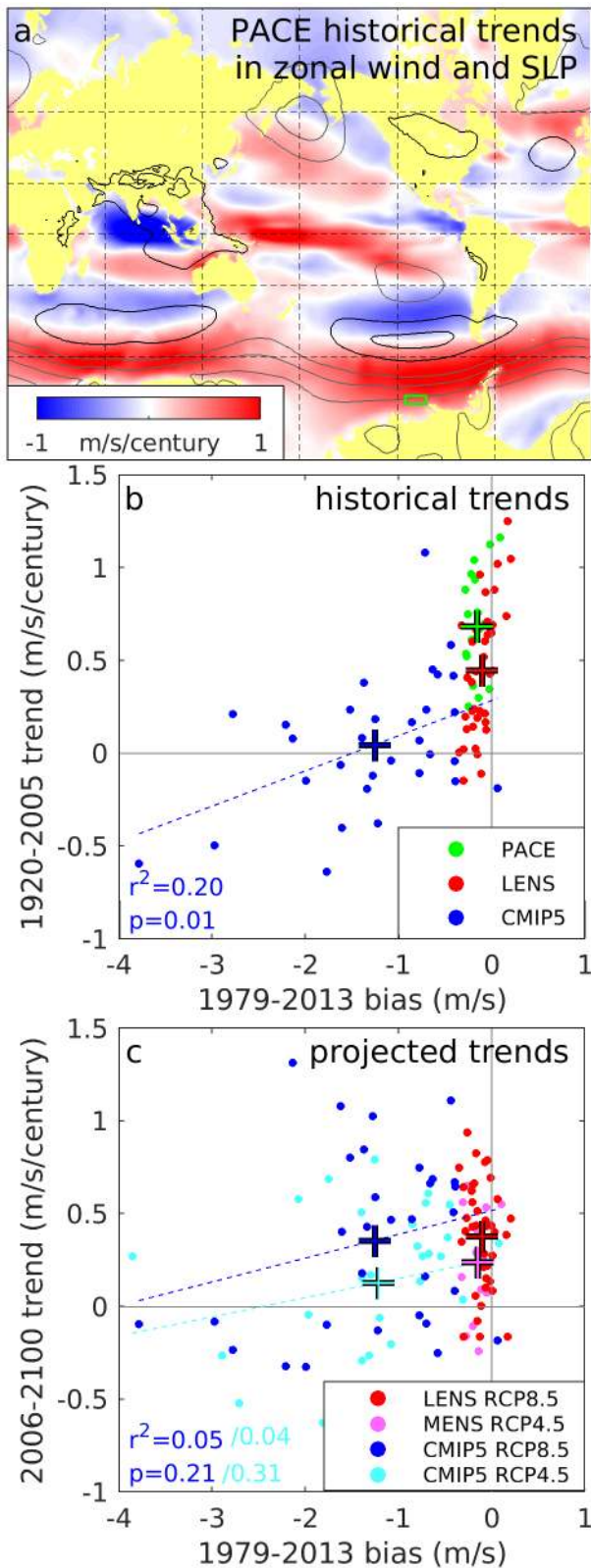
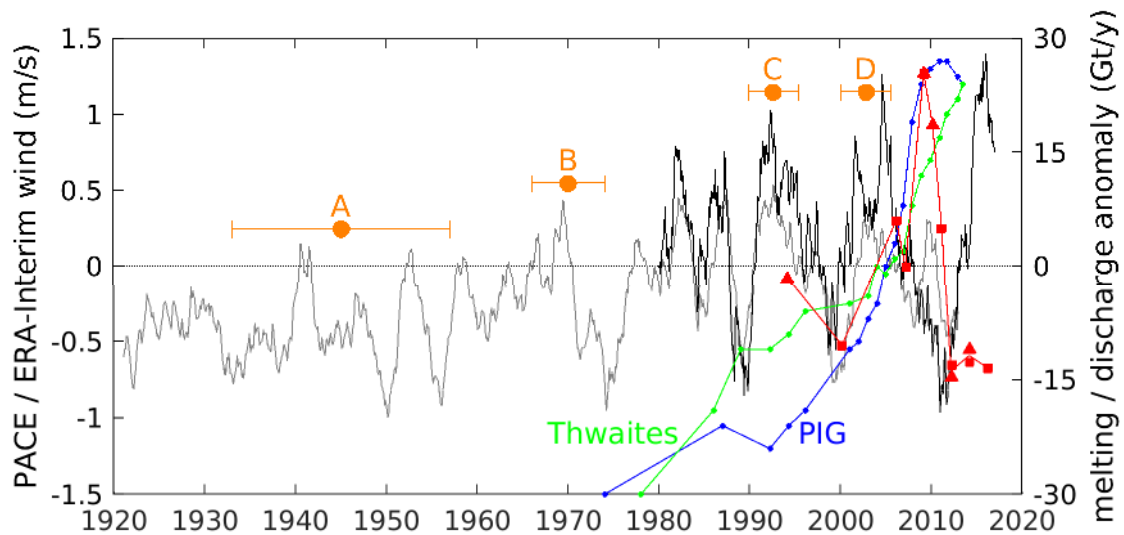


**Figure 4: Trends in Amundsen Sea winds within climate model ensembles.** a) 1920-2005 trends in the PACE ensemble mean. Colours (contours) show trend in zonal winds (SLP). Contours have a spacing of 0.5 hPa/century, with black positive, grey negative, and the zero contour omitted. b) historical and c) projected PITT wind trends versus present-day bias (mean model zonal wind minus mean ERA-Interim zonal wind). Ensemble-mean values are shown by a + symbol. The ensemble regression of CMIP5 historical trends shows that the larger LENS trend is consistent with its smaller bias. There is no dependence of CMIP5 projected trends upon present-day bias.





755

756 **Figure 5: One century of wind forcing and ice-sheet response.** Grey and black show PACE  
 757 ensemble-mean and ERA-Interim winds. Green and blue show anomalies in discharge of  
 758 Thwaites and Pine Island glaciers<sup>3</sup>, relative to 102 and 108 Gt/y median values. Red shows  
 759 anomalies in combined melt rates from Pine Island Glacier<sup>5</sup> (triangles) and Dotson Ice Shelf<sup>6</sup>  
 760 (squares), relative to a median of 48 Gt/y. Orange events include initial (A) and final (B)  
 761 ungrounding of Pine Island Glacier from a submarine ridge<sup>8,12</sup>, and the onset of recent  
 762 thinning of Pine Island (C) and Thwaites (D) glaciers<sup>4</sup> (mean  $\pm 1$  s.d. of dates for tributaries).

763 **Supplementary Tables and Figures**

Name	Description and reference	Time period	Forcing	n	Wind bias (m/s)		
					mean	s.d.	s.e.
PACE	CESM Pacific Pacemaker <sup>56</sup>	1920-2013	historical: radiative + tropical Pacific SSTs	20	-0.16	0.10	0.02
MENS	CESM Medium Ensemble <sup>41</sup>	1920-2080	historical: radiative projected: RCP4.5	15	-0.15	0.11	0.03
LENS	CESM Large Ensemble <sup>30</sup>	1920-2100	historical: radiative projected: RCP8.5	40	-0.11	0.13	0.02
CMIP5 RCP4.5	Coupled Model Intercomparison	1920-2100	historical: radiative projected: RCP4.5	31	-1.21	0.86	0.16
CMIP5 RCP8.5	Project, phase 5 (ref. <sup>31</sup> )	1920-2100	historical: radiative projected: RCP8.5	30	-1.26	0.86	0.16

764 Supplementary Table S1: Description of climate model ensembles considered in this study.

765 The final three columns show statistics of the ensemble member wind biases, calculated

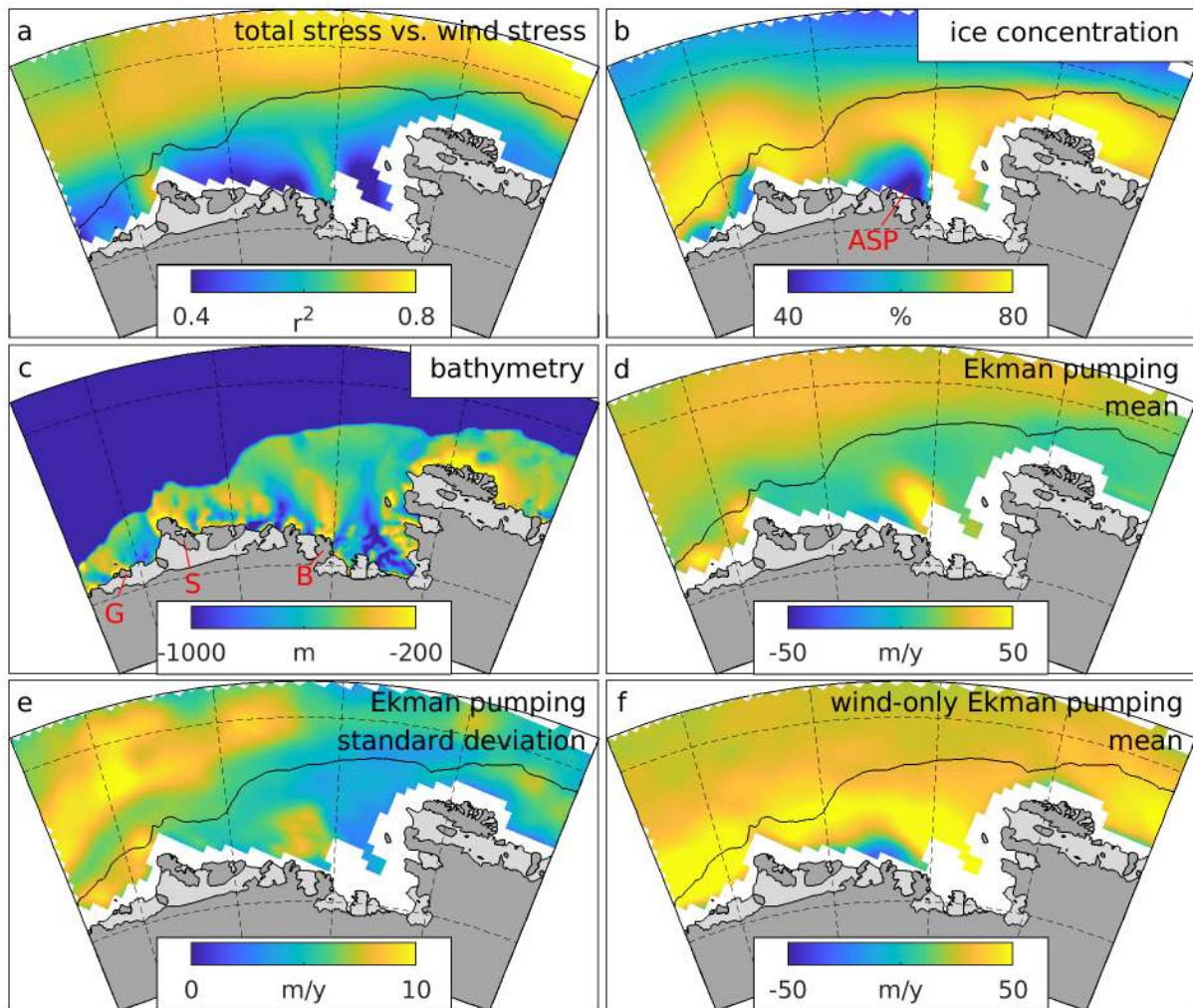
766 relative to ERA-Interim during 1979-2013.

	Summer DJF	Autumn MAM	Winter JJA	Spring SON	Annual
PACE historical 1920-2005	<b><u>0.96 ± 0.47</u></b>	<b><u>0.57 ± 0.86</u></b>	<b><u>0.66 ± 0.60</u></b>	<b><u>0.60 ± 0.55</u></b>	<b><u>0.69 ± 0.27</u></b>
LENS historical 1920-2005	<b><u>1.21 ± 0.61</u></b>	<b><u>0.48 ± 0.57</u></b>	0.07 ± 0.59	0.18 ± 0.69	<b><u>0.45 ± 0.35</u></b>
CMIP5 historical 1920-2005	0.02 ± 0.50	0.01 ± 0.74	0.03 ± 0.72	0.15 ± 0.58	0.05 ± 0.36
MENS RCP4.5 2006-2080	0.03 ± 0.53	<b><u>0.95 ± 0.87</u></b>	<i>-0.28 ± 0.61</i>	0.35 ± 0.80	<b><u>0.24 ± 0.27</u></b>
LENS RCP8.5 2006-2080	0.16 ± 0.64	<b><u>1.14 ± 0.69</u></b>	-0.04 ± 0.94	0.07 ± 0.80	<b><u>0.32 ± 0.45</u></b>
LENS RCP8.5 2006-2100	-0.02 ± 0.45	<b><u>1.49 ± 0.56</u></b>	0.04 ± 0.55	0.05 ± 0.52	<b><u>0.38 ± 0.29</u></b>
CMIP5 RCP4.5 2006-2100	<b><u>0.16 ± 0.43</u></b>	-0.01 ± 0.66	<i>0.30 ± 0.86</i>	0.08 ± 0.76	0.13 ± 0.47
CMIP5 RCP8.5 2006-2100	<b><u>0.32 ± 0.54</u></b>	<b><u>0.56 ± 0.93</u></b>	<b><u>0.41 ± 0.75</u></b>	0.09 ± 0.67	<b><u>0.36 ± 0.48</u></b>

767 Supplementary Table S2: Seasonal trends in the Amundsen Sea wind timeseries. PITT wind  
768 trends are shown as mean ± 1 standard deviation of the distribution of trends in ensemble  
769 members; m/s/century. Trends in italic/bold/bold underline are significantly different from  
770 zero at the 90%/95%/99% confidence level under a one-sample t-test. The seasonal trends  
771 are calculated from seasonal means while, as elsewhere in the paper, the annual trends are  
772 calculated from all monthly data after the application of a 2-year running mean.

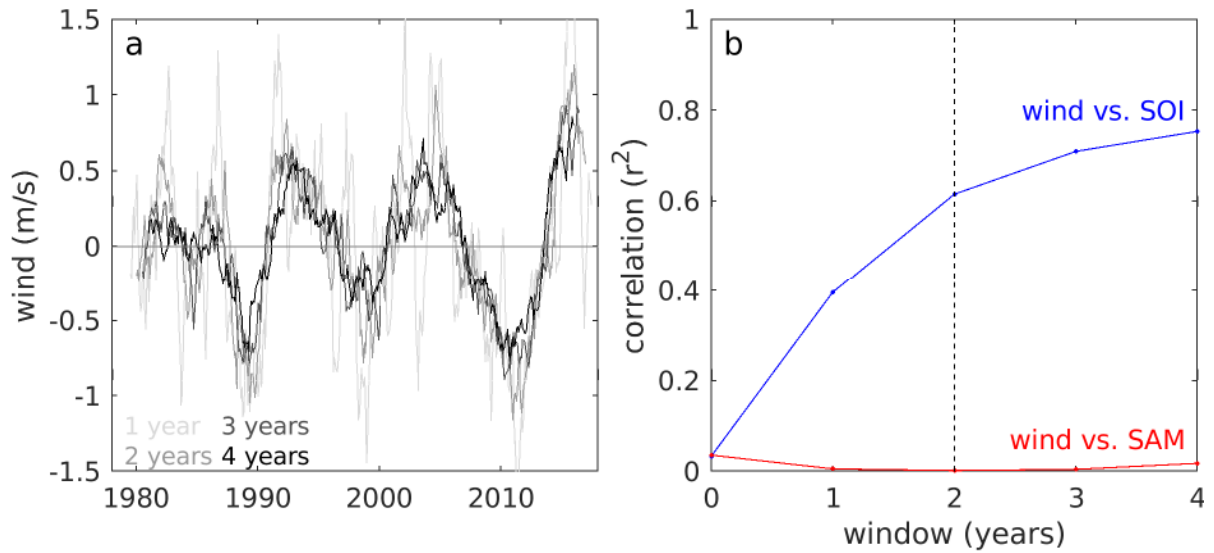
	Summer DJF	Autumn MAM	Winter JJA	Spring SON	Annual
PACE vs. LENS 1920-2005	<i>0.09</i>	0.68	<b><u>0.00</u></b>	<b>0.01</b>	<b><u>0.01</u></b>
LENS RCP8.5 vs. MENS RCP4.5 2006-2080	0.23	0.22	0.14	0.13	0.21
LENS RCP8.5 vs. MENS RCP4.5 2006-2100	0.37	<b>0.02</b>	<b>0.04</b>	<i>0.10</i>	<i>0.05</i>
CMIP5 RCP8.5 vs. CMIP5 RCP4.5 2006-2100	0.10	<b><u>0.00</u></b>	0.30	0.48	<b>0.03</b>

773 Supplementary Table S3: Inter-ensemble differences in trends. The stated values are the p  
774 value of a two-sample t-test of the differences between ensemble trend distributions. Values  
775 in italic/bold/bold underline are sufficient to reject the null hypothesis at the 90%/95%/99%  
776 confidence level. For PACE vs. LENS, the null hypothesis is that the ensemble mean trends are  
777 equal, a two-tailed test. For the projection comparisons, the null hypothesis is that the mean  
778 RCP8.5 trend is no higher than the mean RCP4.5 trend, a one-tailed test.



779

780 Supplementary Figure S1: Details of surface stress on the Amundsen Sea, calculated from  
 781 ERA-Interim reanalysis winds and satellite-tracked sea ice drift (Methods). a) Vector  
 782 correlation between total stress and wind-only stress, calculated using monthly anomalies  
 783 from seasonal climatology (Methods). b) Mean sea ice concentration. c) Bathymetry. d) Mean  
 784 Ekman pumping calculated from total stress. e) Standard deviation of Ekman pumping  
 785 calculated from total stress (after 2-year running mean). f) Mean Ekman pumping calculated  
 786 from wind-only stress. ASP: Amundsen Sea Polynya, G: Grant Island, S: Siple Island, B: Bear  
 787 Island. All quantities are shown over 1992–2016.



788

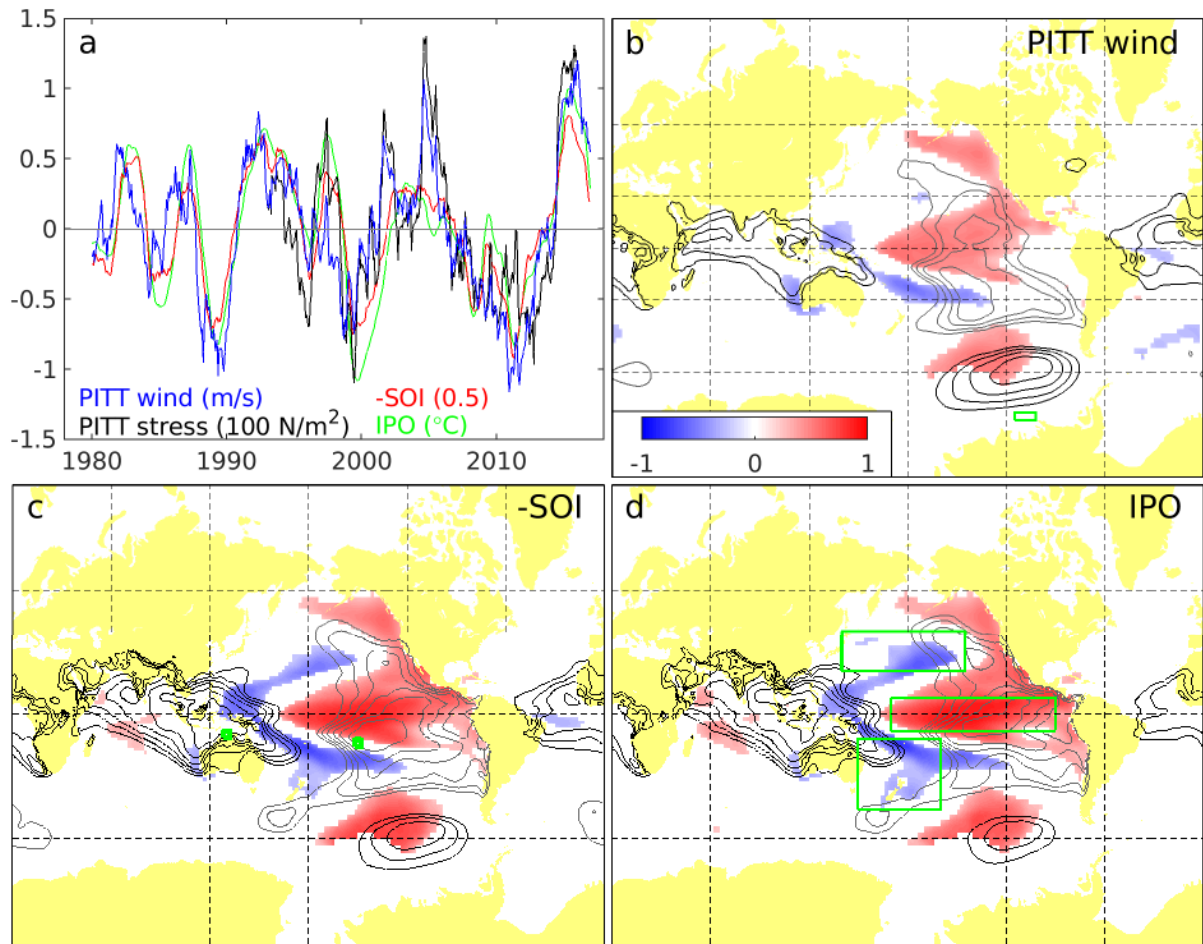
789 Supplementary Figure S2: Dependence of Amundsen Sea wind variability upon running-mean

790 window. a) PITT wind timeseries after smoothing with running means of different window

791 lengths. b) Correlation of PITT wind to Southern Oscillation Index (SOI) and Southern Annular

792 Mode (SAM) indices, as a function of running-mean window length. All time series are

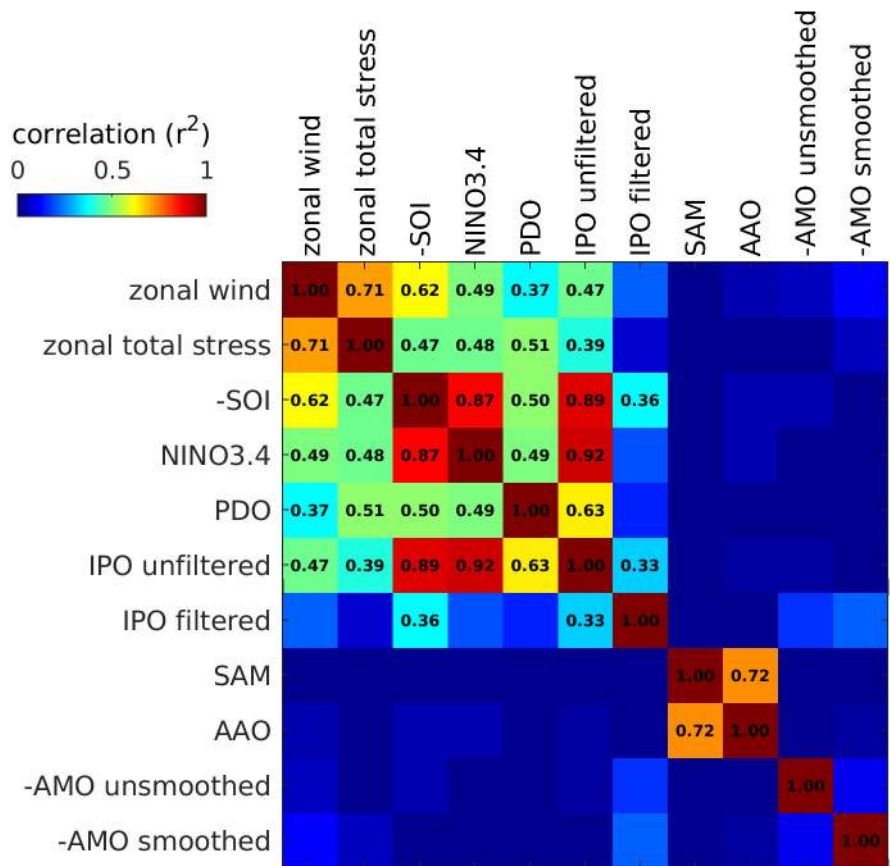
793 detrended.



794

795 Supplementary Figure S3: As Figure 2, but with all correlations insignificant at the 95%

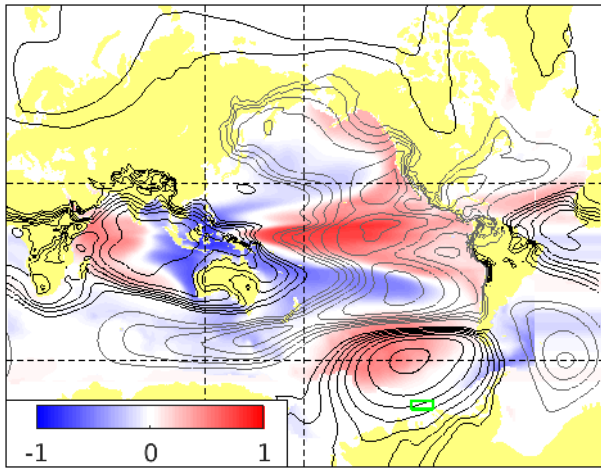
796 confidence level removed from panels b-d. See Methods for details of the significance testing.



797

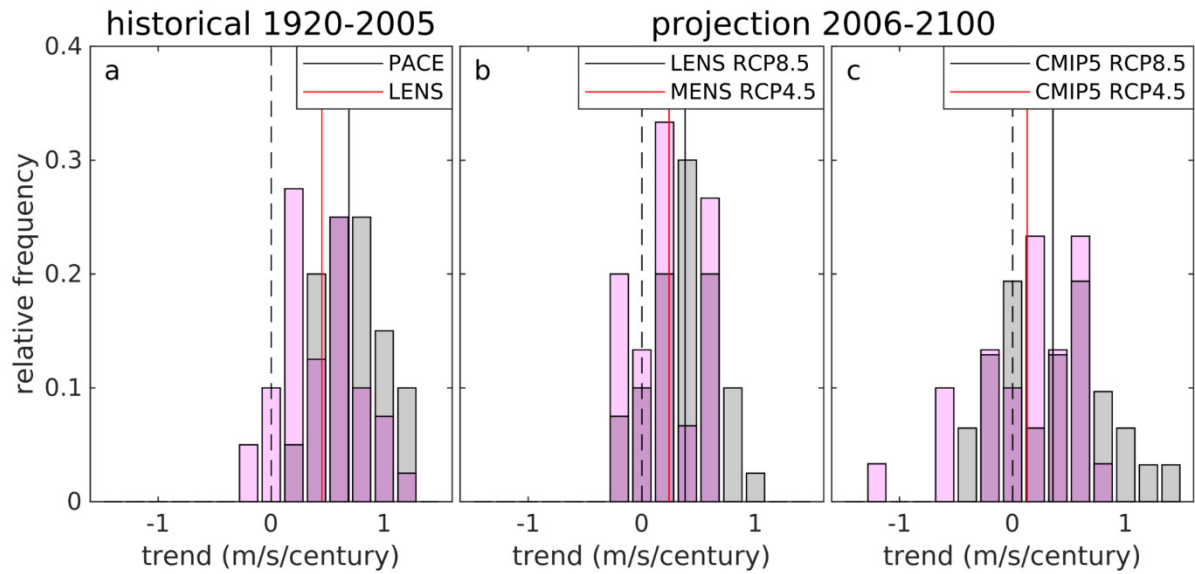
798 Supplementary Figure S4: Correlation between Amundsen Sea winds and climate indices  
 799 (Methods). Only data available during 1979–2017 are used. All timeseries have a 2-year  
 800 running mean applied and are detrended. The  $r^2$  value is given for all correlations significant  
 801 at the 95% confidence level (Methods) SOI: Southern Oscillation Index; PDO: Pacific Decadal  
 802 Oscillation; IPO: Interdecadal Pacific Oscillation; SAM: Southern Annular Mode; AAO:  
 803 Antarctic Oscillation; AMO: Atlantic Multidecadal Oscillation.





804

805 Supplementary Figure S5: Linkages between Amundsen Sea winds and global sea-surface  
806 temperature and sea-level pressure within the PACE ensemble. The plotting is identical to  
807 Supplementary Figure S3b, but for the PACE ensemble mean during 1920—2005. Relative to  
808 Supplementary Figure S3b, the longer period of data availability means that lower  
809 correlations are significant.



810

811 Supplementary Figure S6: Histograms of trends within the members of each ensemble. Solid

812 vertical lines denote the ensemble means. Within each ensemble, each member's trend is

813 equally plausible, so the spread in trends quantifies the uncertainty in the historical and

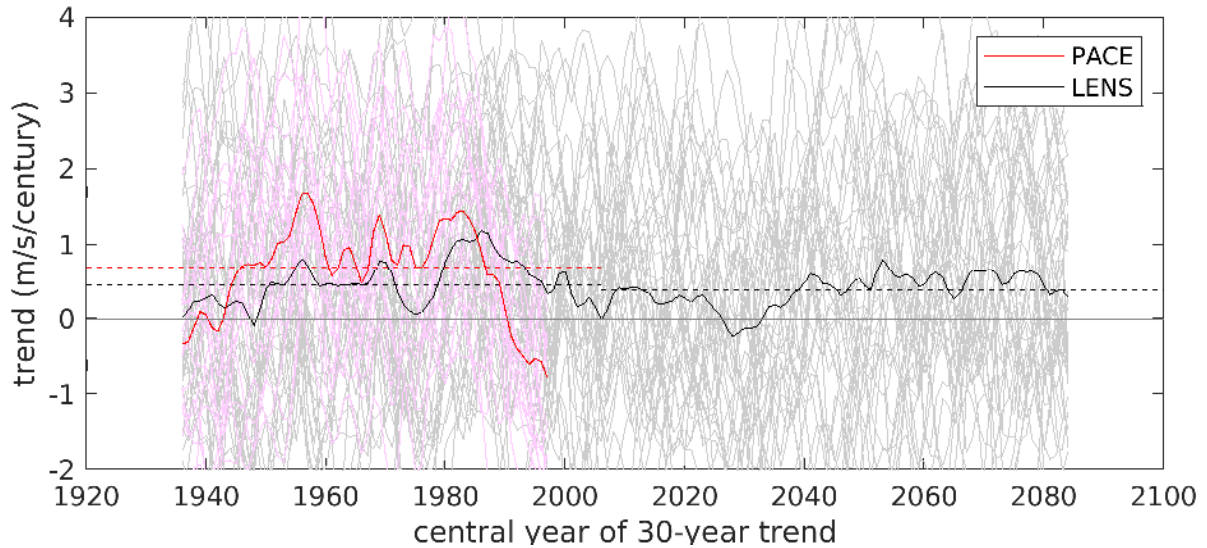
814 projected trends. Members of the PACE, LENS, and MENS ensembles all use the same model,

815 so their ensemble spread is caused by internal climate variability. The CMIP5 ensembles

816 include many different models, so their larger ensemble spread is caused by both internal

817 variability and model structural uncertainty. Note that the MENS trend is calculated over

818 2006-2080.



819

820 Supplementary Figure S7: Evolution of trends in Amundsen Sea winds within the PACE and

821 LENS ensembles. Red and black solid lines show rolling 30-year sub-trends for the ensemble

822 means from PACE and LENS, respectively. Pink and grey lines show trends for the individual

823 ensemble members. Red and black dashed lines show the long-term (1920-2005 and 2006-

824 2100) ensemble-mean trends (Table 1). The trend variation is not smooth as a result of

825 decadal variability, intra-ensemble spread, and historical variability in natural radiative

826 forcings.